LCLS INJECTOR LASER PROFILE SHAPING USING DIGITAL MICROMIRROR DEVICE

S. Li*, S. Alverson, D. K. Bohler, A. Fry, S. Gilevich, Z. Huang A. Miahnahri, D. Ratner, J. Robinson, F. Zhou, SLAC National Accelerator Laboratory, Menlo Park, USA

Abstract

In the Linear Coherent Light Source (LCLS) at SLAC, the injector laser plays an important role as the source of the electron beam for the Free Electron Laser (FEL). The emittance of the beam is highly related to the transverse profile of the injector laser. Currently the LCLS injector laser has undesired features, such as hot spots, which carry over to the electron beam. These undesired features increase electron emittance, degrade the FEL performance, and complicate operations. The injector laser shaping project at LCLS aims to produce arbitrary electron beam profiles, such as cut-Gaussian, uniform, and parabolic, and to study the effect of spatial profiles on beam emittance and FEL performance. Effectively it also allows easy transition between the two spare lasers, where the operators can use the spatial shaper to achieve identical profiles for the two lasers. In this paper, we describe the experimental methods to achieve laser profile shaping and electron beam profile shaping respectively, and demonstrate promising results.

INTRODUCTION

The injector laser at LCLS consists of a Ti:Sapphire laser system, producing a 2 ps pulsed laser at 760 nm with a repetition rate of 120 Hz. The infrared laser is then converted to ultraviolet wavelength (253 nm) via nonlinear process in a frequency tripler. The UV laser then strikes a copper photocathode which emits photo-electrons due to the photo-electric effect [1]. Past studies have shown that certain laser profiles lead to lower electron beam emittance [2, 3]. Figure. 1 is a typical example of the transverse profile of the LCLS injector laser (left) and electron beam profile (right) near cathode. Hot spots and non-uniformities in the laser profile and photocathode quantum efficiency lead to non-uniformities in the electron beam. Therefore, with spatial shaper optics, we can address and remove the non-uniformities and achieve arbitrary profiles.

In this paper, we briefly discuss the hardware choice and experimental setup. We describe the experimental methods to achieve accurate shaping of the laser and the electron beam profiles. We also demonstrate promising results obtained at LCLS.

HARDWARE AND EXPERIMENTAL SETUP

There are many commercially available adaptive optics. J. Maxson et al. [4] have used liquid-crystal-on-silicon (LCoS) spatial light modulators (SLM) to spatially modulate laser and electron beam with the green photocathode at Cornell. However, LCoS based SLMs are not compatible with UV lasers for our case. A. Halavanau et al. [5] have used a microlens array to experimentally characterize and shape the beam transverse profile. Other relevant studies can be found in [6, 7, 8]. After extensive damage tests on various materials [9], we choose to work with digital micromirror device (DMD) from Texas Instruments [10]. Unfortunately, there is no DMD available to work in deep UV as our laser wavelength, so we resort to a third-party company for replacing the window on the chip in order to transmit UV. Damage tests have shown that a converted UV DMD can sustain up to 90 μJ laser power with beam size 1 cm (damage threshold varies with beam size), when the laser pulse is placed after the micromirrors have just stabilized into a new state for each period (see details in [10]).

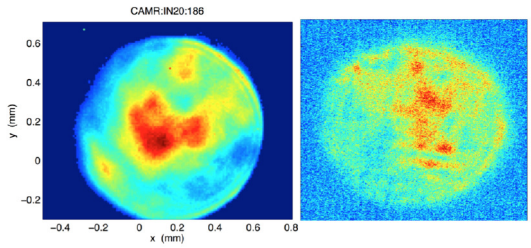

Figure 1: Example of LCLS injector laser transverse profile (left). Example of electron beam emission profile (right) near cathode.

The model we use is DLP 7000 DMD which consists of 768×1024 micromirrors with size 13.68 μm. The micromirrors can flip into two states, ON or OFF corresponding to +/-12 °, given an input voltage. Due to the nature of the DMD design, laser intensity reduction is achieved by grouping the individual micromirrors into macropixels and turning off a fraction of randomly-distributed micromirrors in each macropixel to reduce intensity by a certain amount. The device is programmable through an API in Matlab, which we incorporate into the LCLS EPICS control system.

A technical subtlety is the pulse front tilt introduced by the DMD, as from a grating. The pulse front tilt is effectively a correlation between the time coordinate and the transverse position coordinate. In the case of the DMD, or a grating, the correlation results in an elongated pulse length. We compensate this effect by introducing a diffraction grating upstream of the DMD (Fig. 2), which cancels the pulse front tilt from the DMD. The compensation is confirmed by measuring the electron bunch length in comparison to the regular setup without DMD, which shows < 10% difference.

* siqili@slac.stanford.edu

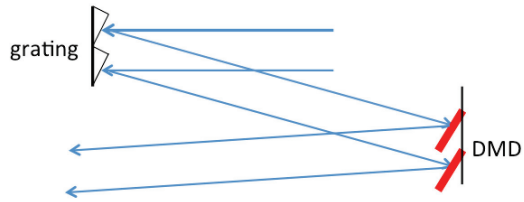

Figure 2: Grating and DMD setup in order to compensate pulse front tilt introduced by the DMD.

SHAPING THE LASER

Mapping

In the optical setup, the DMD plane is imaged on to the cathode. A Virtual Cathode Camera (VCC) reflects the laser profile on the cathode, and we treat VCC as the target plane for shaping the laser. In order to achieve accurate shaping we need to have a mapping between the DMD plane and the VCC plane. We assume a linear transformation between the two planes, which takes into account of magnification, rotation, skewing, and mirror imaging [4]. This transformation is illustrated in Fig. 3 and the transformation relation can be expressed by a set of linear equations (Eq. 1).

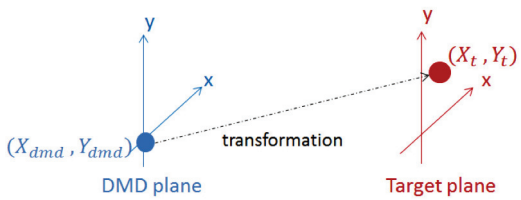

Figure 3: Mapping between the DMD plane and target plane (VCC in our case).

$$\begin{aligned} X_t &= C_x(1)X_{dmd} + C_x(2)Y_{dmd} + C_x(3) \\ Y_t &= C_y(1)X_{dmd} + C_y(2)Y_{dmd} + C_y(3) \end{aligned} \quad (1)$$

We turn on a small section of DMD at (X_{dmd}, Y_{dmd}) and record the signal position on the target plane (X_t, Y_t). We repeat the procedure at least three times and apply a least square fitting to solve for the C coefficients from the set of equations to obtain the mapping relation. This method can be used in any target plane as long as the imaging process is linear. As a demonstration of the mapping, we put a Stanford tree on DMD, targeting the VCC plane, as shown in Fig. 4.

Shaping

We implement an algorithm that iteratively shapes the laser. The user initially provides a general choice of target shape, such as flat-top, cut-Gaussian, or parabolic. Considering that the DMD only reduces intensity, the user also provides a minimum efficiency required for shaping. The first iteration defines a cost function in terms of shaping error and shaping efficiency, which is then minimized to find the optimal parameters that specifically determine the goal shape. The shaping gain is defined as the ratio of the number of real micromirrors to turn off to the calculated number of micromirrors to turn off. We allow for gain less than 1 and multiple iterations to approach the target shape. So far, we have demonstrated preliminary laser shaping to test the algorithm (Fig. 5).

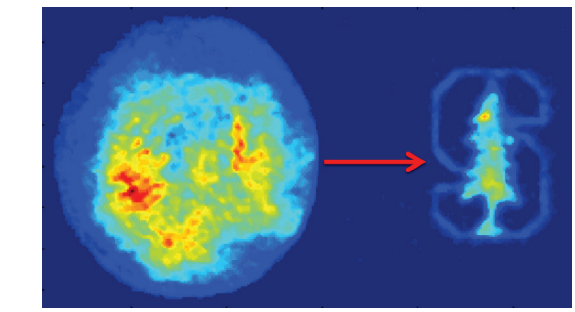

Figure 4: Original beam profile at VCC (left) and Stanford tree profile at VCC (right).

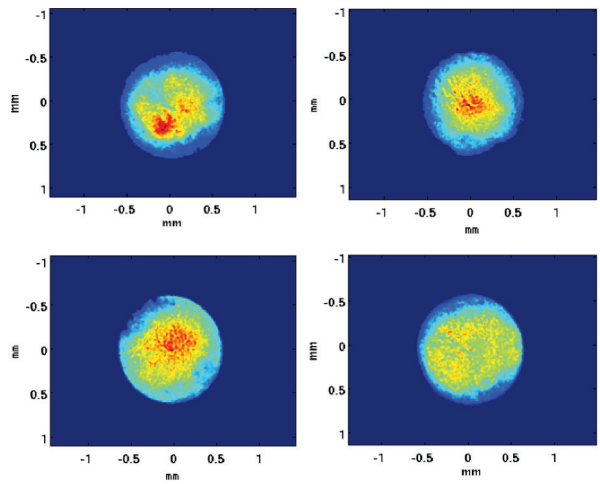

Figure 5: Example VCC images of laser shaping. Top left is the original laser profile. Top right is parabolic shaping. Bottom left is cut-Gaussian shaping. Bottom right is flat-top shaping.

Due to the grating nature of a DMD, the micromirrors diffract the beam into different orders. The optical set up was designed to output most efficiency into a central diffraction order with 60% efficiency. Considering the grating efficiency and transport efficiency, we expect 10 to 15% total efficiency. With 90 μJ on the DMD limited by damage threshold, this corresponds to 12 μJ on cathode. With shaping, we have operated with 90 to 130 pC of charge so far. Since we are mostly limited by DMD damage threshold, the final charge can be increased by custom-made DMD that can sustain higher laser power at deep UV.

SHAPING THE ELECTRON BEAM

Compared to shaping the laser, the complication of shaping the electron beam comes in mapping. The electron

imaging from cathode to a downstream image plane is not linear as in the optical case. For example, the magnification depends on the charge, which again depends on the quantum efficiency (QE) of the cathode, and quantum efficiency nonuniformity is what we are trying to correct for by shaping the electron beam profile. Therefore, instead of following the mapping procedure as in the laser shaping case, we choose the target plane immediately after cathode, where the electron emission profile is the product of the laser profile and the QE profile of the cathode.

In order to obtain a QE profile, we need to measure charge counts across the area where the laser strikes the cathode surface. Since we only need a relative QE map, we use a YAG screen downstream of the cathode to capture electron emission. The total count of the signal is a measure of charge. We turn on a 30 by 30 micromirrror square on DMD and move it across the laser profile. For each square, we analyze the YAG image to measure the charge count. At the same time we analyze the VCC image to measure laser intensity. The procedure of the raster scan is illustrated in Fig. 6. The mapping between (X_{dmd}, Y_{dmd}) and (X_t, Y_t) is also obtained during the scan. To avoid measurement and analysis bias which leads to correlation between measured QE and laser intensity, each time before we start a raster scan, we shape the laser profile into a flat-top beam on VCC, and then apply the flat-top mask together with the square to do the raster scan. In this way, we ensure that the laser intensity is flat across the beam profile and the charge counts on YAG reflect the QE of the cathode. Indeed, the correlation coefficient of the measured QE and laser intensity is < 0.05. We also move the laser around cathode to expand the region of the raster scan and later merge the results together. Figure 7 shows the results from two scans. The resolution of the QE scan is determined by how small a square we can put on DMD while maintaining significant signal to noise ratio on VCC and YAG screens. The lowest resolution we can put on is 30×30 micromirrors squares, taking into account of optical demagnification, which corresponds to an area of 90×90μm on the cathode.

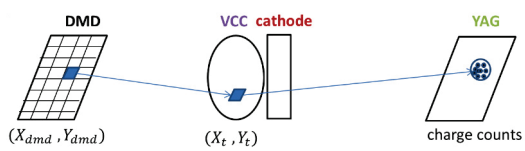

Figure 6: Illustration of raster scan to obtain a QE map across the laser beam area.

With the measured QE we can feed the new input, i.e. the product of laser profile and QE map, to our shaping algorithm as described in the laser shaping section. The experiment is on-going at LCLS.

CONCLUSIONS

In this paper, we have discussed the motivation of injector laser profile shaping at LCLS to control laser and electron beam profile and to study the effect on emittance and FEL performance. We use the digital micromirror device to experimentally shape the transverse laser profile. We described the method to obtain mapping between DMD plane and target plane, and an algorithm to achieve laser profile shaping. For electron beam shaping, we work around the nonlinear nature of electron imaging by reconstructing electron emission from the cathode. We scan small areas across the DMD and measure charge emission to obtain a quantum efficiency profile. We compensate for the measured QE profile by altering the target laser profile, and then use the laser shaping algorithm to control the emitted electron beam. Currently we are developing more accurate electron beam imaging in order to assess the result of shaping. We are also connecting the laser profile to FEL performance by incorporating the shaping process into a Bayesian optimizer [11].

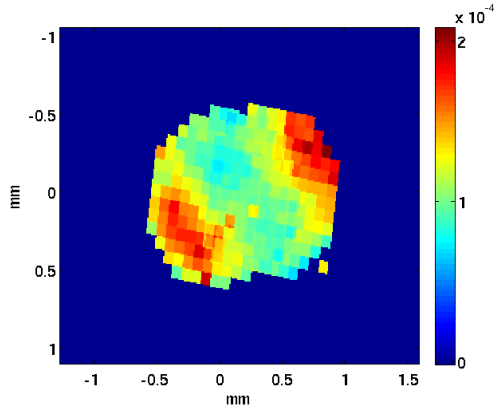

Figure 7: Combined two raster scan results of the QE map.

REFERENCES

[1] Akre, R., et al. "Commissioning the linac coherent light source injector", *Physical Review Special Topics-Accelerators and Beams*, vol. 11.3, p. 030703, 2008.

[2] Zhou, Feng, *et al.,* "Impact of the spatial laser distribution on photocathode gun operation." *Physical Review Special Topics-Accelerators and Beams*, vol. 15.9, p. 090701, 2012.

[3] Brachmann, A., *et al.* ,"LCLS drive laser shaping experiments." in *Proceedings of the International Free-Electron Laser Conference 2009,* Liverpool, UK, pp. 463 - 465.

[4] Maxson, Jared, *et al.*, "Adaptive electron beam shaping using a photoemission gun and spatial light modulator." *Physical Review Special Topics-Accelerators and Beams*, vol. 18.2, p. 023401, 2015.

[5] Halavanau, A., *et al.*, "Microlens Array Laser Transverse Shaping Technique for Photoemission Electron Source." *arXi,v preprint arXiv:1609.01661,* 2016.

[6] Rublack, T., *et al.* ,"Design of a Spatio-temporal 3-D Ellipsoidal Photocathode Laser System for the High Brightness Photoinjector Pitz.", in *Proceedings of the International Free-electron Laser Conference 2014,* Basel, Switzerland, pp. 878 - 880.

[7] Musumeci, P., *et al.*, "Experimental generation and characterization of uniformly filled ellipsoidal electron-beam distributions.," *Physical Review Letters*, vol. 100.24, p. 244801, 2008.

[8] Matsui, Futoshi, *et al.*, "Genetic-algorithm-based method to optimize spatial profile utilizing characteristics of electrostatic actuator deformable mirror," *Optical Review, vol.* 15.3, pp. 156-161, 2008.

[9] Li, S., *et al.*, "LCLS injector laser modulation to improve FEL operation efficiency and performance," in *Proceedings of IPAC2015, Richmond, VA*.

[10] Hornbeck, L. J. ,"Digital Light Processing and MEMS: Timely Convergence for a Bright Future (Invited paper)," in *Proceedings SPIE. Vol. 2639.*

[11] McIntire, Mitchell, *et al.*, "Bayesian Optimization of FEL Performance at LCLS," in *7th International Particle Accelerator Conference (IPAC'16),* Busan, Korea, May 2016.